

COMPARISON OF ARTIFACT REMOVAL TECHNIQUES ON SINGLE-TRIAL EVENT-RELATED POTENTIALS FOR USE IN BRAIN-COMPUTER INTERFACES

ALESSANDRO B. BENEVIDES*, TEODIANO F. BASTOS FILHO†, MÁRIO SARCINELLI FILHO‡

**Departamento de Engenharia Elétrica, Universidade Federal do Espírito Santo, Av. Fernando Ferrari, 514, Goiabeiras, Vitória, Brasil*

Emails: sandrobotti@gmail.com, teodiano@ele.ufes, mario.sarcinelli@ele.ufes.br

Abstract— This paper presents a comparison of four artifact removal techniques on single-trial event-related potentials (ERPs). The techniques analyzed are the threshold analysis, the filtering approach and the Independent Component Analysis (ICA). Two algorithms that are based on two broadest definitions of independence for ICA were tested, which are the *fastICA* and *runica*. The processing time of the techniques, the electroencephalographic (EEG) signal-to-noise ratio (SNR) and the event-related desynchronization/synchronization (ERD/ERS) are studied during four motor mental tasks, which are the imagination of either movement of right and left hands, both feet and rotation of a cube. In order to estimate the number of epochs necessary to observe the ERD/ERS pattern and to compare the performance of the artifact removal techniques, we suggest an analysis of the EEG SNR through a comparison with the correlation between the ongoing average and the final ERD/ERS curve. The *fastICA* algorithm obtained the best performance among the analyzed techniques. It improved the EEG SNR and it increased the ERD/ERS amplitude by $12.6 \pm 9.4\%$. The *fastICA* algorithm spent 1 ± 0.18 ms and it is the best option to be implemented online for artifact removal in BCI applications.

Keywords— Artifact removal, Independent component analysis, Single-trial event-related potentials, Event-related desynchronization/synchronization, Brain-computer interfaces.

1 Introduction

Recent studies have succeeded in demonstrating that non-invasive measures, such as the electroencephalographic signal (EEG), may be used to control robotic devices (del R. Millan et al., 2004; Ferreira et al., 2008; Muller et al., 2010), using specific interfaces between a computer and the human brain. For a detailed review on such interfaces, referred to as Brain-Computer Interfaces (BCIs), see (Wolpaw et al., 2002; Wolpaw, 2007; Cincotti et al., 2008).

In the context of BCI usage, this work aims at improving a BCI reliability by increasing the EEG signal-to-noise ratio (SNR). Here, "noise" includes non-phase-locked EEG signals and non-neural artifacts such as eye blinks and eye movements. The simplest approach to deal with the artifact is to perform a threshold analysis (Croft and Barry, 2000; Jung et al., 2000). Some more complex approaches include performing Blind Source Separation (BSS) using Independent Component Analysis (ICA). Two algorithms that are based on two broadest definitions of independence for ICA were tested, which are the *fastICA* and *runica* (Jung et al., 2001; Ford et al., 2004). The processing time of the studied techniques are presented in order to evaluate whether it is possible to adapt the algorithms to an online approach.

In order to estimate the number of epochs necessary to observe the event-related desynchronization/synchronization (ERD/ERS) pattern and to compare the performance of the artifact removal techniques, we suggest an analysis of the EEG SNR through a comparison with the correlation between the ongoing average and the final ERD/ERS curve.

2 Materials and Methods

2.1 Experimental environment

Data were acquired with five right handed male subjects aged between 26 to 34 years (30.4 ± 3.5). All subjects had normal hearing, normal or corrected-to-normal vision and no history of substance abuse, major medical psychiatric illness, or developmental or neurological disorder.

The BrainNet36[®](BNT) device was used for EEG acquisition with a cap of integrated electrodes from MedCap[®] company. We used 19 electrodes positioned according to the international 10-20 system. The grounding electrode was positioned on the user forehead, monoauricular reference was adopted and all impedances were kept below 5 K Ω (Ford et al., 2004; Luck, 2005). The EEG was acquired at a sampling rate of 200 Hz. BNT is a device for clinical purposes that does not export data online. Therefore, a sniffer programmed in ANSI C was developed to export these data allowing the online processing, which was performed on MATLAB 7.11.0[®] (R2010b) in an Intel[®] Core™ i7 computer.

For each mental task 60 epochs were taken, each epoch corresponding to 25 s. For each epoch subjects were instructed to sit with hands resting on the legs and to observe a cross in the center of the screen. The cross is a fixation point to avoid excessive eye movement artifact. After 5 s an arrow replaces the cross indicating the start of the mental task. The mental task lasts 10 s, and then the cross reappears in place of the arrow indicating that the mental task is over. The subject must remain static until the cross is replaced by a circle at time 25 s, indicating the end of the record.

The project was approved by the Ethics Committee of the Universidade Federal do Espírito Santo (Brazil), recognized by the Ethics Committee of the Research Ethics National Commission (CEP-048/08).

2.2 EEG pre-processing

The study of spatial filters presented by (McFarland et al., 1997) concluded that the Common Average Reference (CAR) and large Laplacian methods would be suitable for BCIs based on the paradigm of motor imagination. Large Laplacian method uses electrodes with 6 cm of distance one from each other. The motor cortex has radius between 6 to 12 cm, then Laplacian filters over the motor cortex with radius smaller than 6 cm would attenuate the information from the motor cortex itself. The present study used different motor related tasks, and as we do not know the exact size of the brain areas that are active during the mental tasks, the CAR method was adopted.

2.3 Description of the ERD/ERS method

The ERD/ERS pattern is extensively discussed in (Pfurtscheller and da Silva, 1999) and will be briefly covered below. During no specific mental task, individual neurons of a neural mass became synchronized with the thalamic pacemaker signal. Then, the neuron mass emits signals in a specific frequency band. Thus, the resulting EEG of the neural mass has higher energy in frequency bands corresponding to the synchronization. Conversely, during the mental task individual neurons of a neuron mass lose the synchrony, emitting signals at different frequencies, which are specific to perform the mental task. Therefore, the EEG energy of the neural mass is lower for frequency bands corresponding to the synchronization.

Then, the ERD and the ERS are, respectively, the relative decrement and increment of energy that occurs in specific frequency bands. During the mental task an ERD can be observed, which is followed by an ERS when the mental task is over. Figure 1 shows the application of the classic method for measuring the ERD/ERS pattern, as described by Pfurtscheller et al. (1999), for subject 3 (26 year old).

Due to the large amount of noise present in the EEG signal, the ERD/ERS pattern is better observed in the average behavior obtained from several trials. It is considered that the ERD/ERS pattern is time-locked to the event and the spontaneous EEG activity is modeled as an additive random noise. As the number of trials increases the time-locked activity stresses and the spontaneous activity decreases, then the ERD/ERS pattern can be observed.

The EEG obtained in each trial, under the same conditions, is called epoch. In this exper-

iment 60 epochs were used and the subject performed the mental task of imagination of movement of the right hand. Figure 1(a) shows in gray the superimposition of the EEG from channel C3 of the first, fifteenth, and thirtieth epochs, respectively, in black, dark and light gray. The mental task lasted 10 s, occurring between 5 and 15 s of the EEG record, which corresponds to the central area, not hatched of the figure. The voluntary motility is 100 % crossed, therefore, channel C3, positioned over motor cortex of the left brain hemisphere, was used in the analysis of the EEG concerning the imagination of the movement of the right hand.

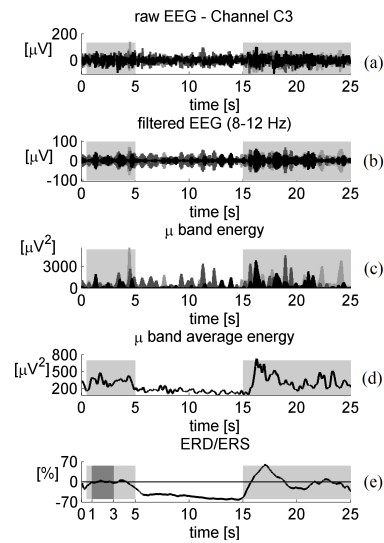


Figure 1: ERD/ERS calculation method. (a) raw EEG from channel C3 during the first, fifteenth, and thirtieth epoch, respectively in black, dark and light gray; (b) EEG from channel C3 filtered at μ band; (c) channel C3 μ band energy (d) channel C3 μ band average energy of 60 epochs; (e) channel C3 μ band ERD/ERS.

Then, EEG signals from channel C3 were filtered in specific band of frequencies. For motor mental tasks, it is known that the ERD/ERS occurs in μ (8-12 Hz) and β (14-30 Hz) frequency bands (Pfurtscheller and da Silva, 1999). Figure 1(b) shows the EEG filtered at μ band. In this study we used a FIR equiripple bandpass filter with forward and reverse order filtering algorithm to cancel the effect of phase distortion. This figure also shows the superimposition of the filtered EEG of the three aforementioned epochs. Our objective with this figure is not to show individual characteristics of the epochs, but just to emphasize that the steps are performed individually, for each epoch.

The filtered EEG from each epoch was squared in order to obtain the signal energy (figure 1(c)). Then, the average energy of all epochs was calculated (figure 1(d)). Here, the signal en-

ergy is used to prevent the cancellation of positive and negative EEG amplitudes during the average process.

Finally, as the ERD/ERS are measured as percentages, the average energy of a previous reference period is calculated. Thus, the signal energy can be measured in relation to the reference period. In this work, the reference period is the one between 1 s and 3 s of the recording, which is highlighted in figure 1(e) as the interval shaded in dark gray. The horizontal line stresses the null value of the reference period.

In figure 1(e) the energy decrement of around 70 % occurring between 5 s and 15 s is the ERD, and the energy increase of around 60 % occurring between 15 s and 20 s is the ERS. Therefore, the ERD/ERS pattern can be observed mainly at electrodes placed over the scalp region of motor cortex during motor mental tasks.

3 Independent component analysis

ICA is a method for solving the BSS problem recovering N independent source signals, \mathbf{s} , from N linear mixtures, \mathbf{x} , and it relies on the assumption that the source signals are mutually statistically independent or decorrelated while their mixtures are not. Statistical independence requires that all second-order and high order correlations are zero, while decorrelation only seeks to minimize second-order statistics, which are the covariance or correlation. The linear mixture of N sources can be written as,

$$\mathbf{x} = \mathbf{A} \cdot \mathbf{s} \Leftrightarrow \mathbf{s} = \mathbf{A}^{-1} \cdot \mathbf{x} \Leftrightarrow \mathbf{s} = \mathbf{W} \cdot \mathbf{x} \quad (1)$$

Where, \mathbf{A} is an unknown invertible square matrix given by an ICA algorithm. Once \mathbf{A} is known, the source signals can be found by inverting the mixing process, leading to the "unmixing" matrix \mathbf{W} . The rows of the input matrix \mathbf{x} are EEG signals recorded at different channels and its columns are measurements recorded at different time points. The columns of the source matrix \mathbf{s} contain the time course of ICA components. The columns of \mathbf{A} gives the relative projection strengths of the respective ICA components at each EEG site. These scalp weights represent the fixed scalp topography of each ICA component, and it provides evidence for the component physiological origin. For example, electrooculography (EOG) and blink artifacts should project mainly to frontal sites, then the ICA components with high weight projected to frontal sites, should be related to this kind of artifact, that can also be verified in the time course of the component.

Then, the ICA components related to artifacts can be set to zero and artifact-free signals can be obtained projecting non-artifactual ICA components back onto the scalp (Jung et al., 2000;

Jung et al., 2001). The artifact-free EEG signals, \mathbf{x}_0 , can be obtained from the artifact-free source matrix, \mathbf{s}_0 , and the mixing matrix \mathbf{A} , by $\mathbf{x}_0 = \mathbf{A} \cdot \mathbf{s}_0$.

4 Results

4.1 Applying threshold analysis and filtering for artifact removal

Figure 2 shows a 25 s single-trial of subject 2 contaminated by five eye blink artifacts. Below each channel (Fp1 and C3) it is the periodogram. This figure shows the raw EEG, the application of the CAR method, the discard of artifacts by using the threshold analysis and the filtering method. For the threshold analysis whenever EEG signals from selected frontal channels exceed $\pm 50\mu\text{V}$, a 0.5 s time window centered around the EEG peak of these electrodes will be discarded or annulled in all EEG channels (Croft and Barry, 2000; Jung et al., 2000). In the filtering approach the corrupted time window identified by the threshold analysis is replaced by a filtered one. The filtered time window used a FIR equiripple highpass filter set to 5 Hz, with forward and reverse order filtering algorithm.

It can be noted in channel C3 that using the threshold and the filtering approaches a peak of activity around 10 Hz becomes evident between 15 and 25 s. And this peak of activity lasts longer for the filtering approach, because the threshold approach causes loss of information.

4.2 Applying ICA for artifact removal

Figure 3 shows the ICA components and their fixed scalp topography of the same trial analysed before, in figure 2. This experiment correspond to the mental task of imagination of movement of the right hand, which occurred between 5 and 15 s, and 19 electrodes were used. Then, the input matrix has 19 linear mixtures and ICA algorithm results in 19 independent components and 19 respectively scalp topographies, that are shown in the right side of each component.

In the scalp topography, the relative strength of the ICA component over the 19 scalp sites is shown in shades of gray, in which light shades are related to a high strength

In the left part of figure 3 it can be seen that the first ICA component (ICA-1) is very similar to the time course of the eye blink artifact shown in the EEG of channel Fp1 in figure 2. The scalp topography of this component is shown at its right side, and it can be seen that its strength is higher for frontal sites, in particular at Fp2. Then, this component can be set to zero in order to obtain a relative artifact-free EEG. The right part of figure 3 shows the minimization of eye blink artifacts by using *fastICA* and *runica* algorithms. It

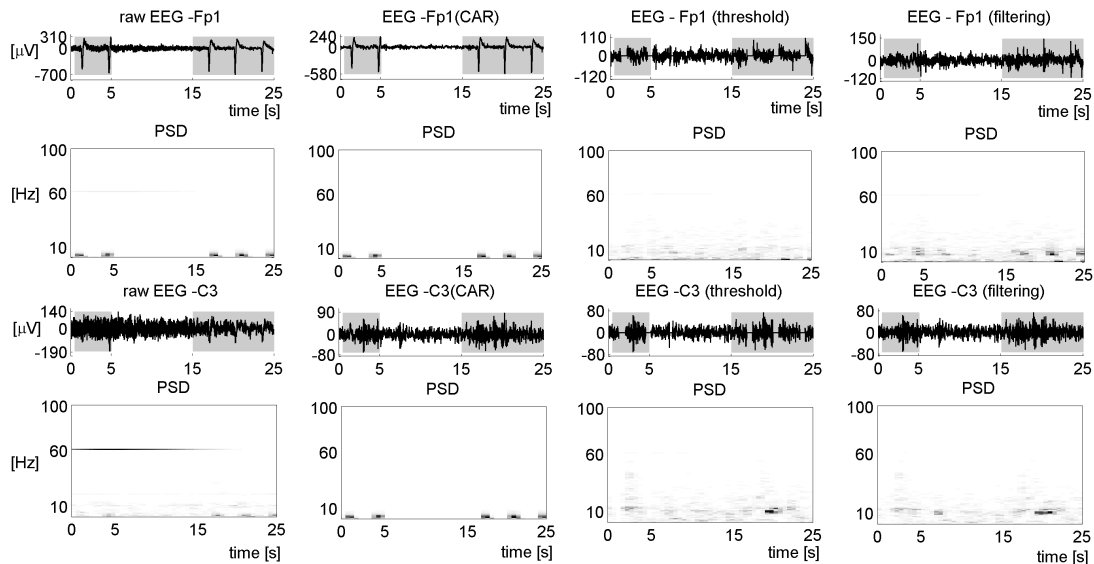


Figure 2: EEG of channels Fp1 and C3 and their periodograms during the application of the following cases: raw EEG; CAR method; threshold analysis and filtering.

can be seen that for both algorithms the eye blink artifacts of channel Fp1 are completely annulled and there is no low frequency artifact in the periodogram. It can be noted in channel C3 a peak of activity around 10 Hz becomes evident between 15 and 25 s.

In average, the threshold analysis spent $0.34 \pm 0.47 \mu\text{s}$. The filtering approach spent 178.6 ± 7.7 ms. The *fastICA* algorithm spent 1 ± 0.18 ms and the *runica* algorithm spent 3.6 ± 0.61 ms.

4.3 ERD/ERS improvement by using ICA

Figure 4 shows ERD/ERS of subject 1 obtained for channel C3 using 60 epochs during mental task of imagination of cube rotation. The black line shows the ERD/ERS obtained without artifact removal, by only using the CAR method. The dark gray line shows the ERD/ERS obtained with *fastICA* and the light gray line shows the ERD/ERS obtained with *runica*. It can be observed that *fastICA* provided a small improvement in the ERD/ERS amplitude. The ERS peak reached 163% and by using *fastICA* it reached 186% while the ERD did not changed.

It can be seen that the *runica* worsened the ERD/ERS curve, and the ERS peak only reached 45%. The average result of applying ICA during all mental tasks and subjects was an improvement of $12.6 \pm 9.4\%$. It means that, in average, the application of *fastICA* enhanced a little the EEG SNR so the ERS peak or the ERD depression was more detectably.

4.4 EEG SNR analysis

The SNR of the EEG approximately increases proportionally to the number of trials and the noise

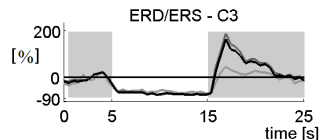


Figure 4: ERD/ERS of channel C3 at μ band. In black: ERD/ERS obtained without artifact removal; in dark gray: ERD/ERS obtained with *fastICA*; in light gray: ERD/ERS obtained with *runica*.

amplitude of the average of N trials is $SNR = 1/\sqrt{N}$ times that of a single trial. Then, an excessive number of trials will not cause meaningful changes in the observed ERD/ERS (Luck, 2005). When dealing with the EEG signal it is very difficult to distinguish the noise component from the clean ERP signal. Then, it is complicated to perform a realistic estimation of the ERP and the noise amplitudes in order to calculate the SNR improvement for each new added trial. Then, we consider using the signal correlation that is strongly related to the SNR. Let's consider the correlation between a signal x with this same signal corrupted with a noise n , and both are zero-mean and uncorrelated. Then, we have that the corrupted signal is given by $y=x+n$, and the correlation is

$$\rho_{x,y} = \frac{S}{\sqrt{S \cdot (S + N)}} \Leftrightarrow \frac{S}{N} = \frac{\rho_{x,y}^2}{1 - \rho_{x,y}^2} \quad (2)$$

Where S is signal energy and N is the noise energy. Equation 2 shows the relation between the SNR and the correlation for the specific case in which both signal and noise are uncorrelated.

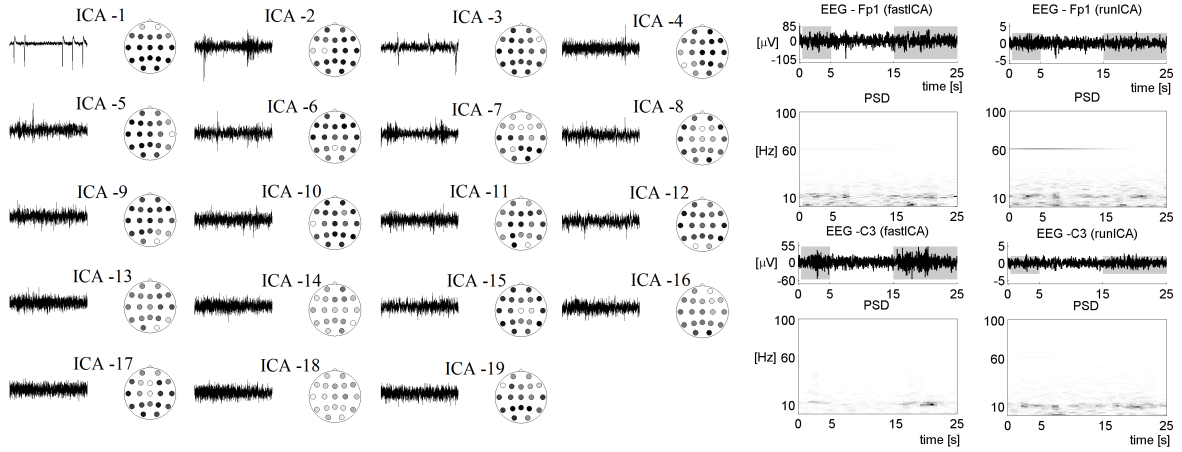


Figure 3: Left: ICA components obtained by *fastICA* algorithm and their fixed scalp topographies; Right: EEG of channels Fp1 and C3 and their periodograms during the application of the following cases: *fastICA* algorithm and *runica* algorithm.

However, the assumption that the ongoing average is uncorrelated from the ERD/ERS curve is not true, and then, eq. 2 cannot be directly applied to find the ERP SNR. As a conservative approach, the rescaled correlation function was compared with the square root of the SNR (i. e., the noise amplitude) by using a polynomial regression.

An estimative of the EEG SNR was performed, using a comparison with the correlation between the ongoing average and the final ERD/ERS curve (c1), and the correlation between a single trial and the ongoing average as well (c2). This analysis was performed in order to estimate if the number of trials used to observe the ERD/ERS was enough or excessive.

The left part of figure 5 shows c1 of channel C3 in the black continuous line, obtained for the right hand mental task. From 30 epochs forth c1 reaches 95% and the ERD/ERS curve obtained so far is very similar to the ERD/ERS curve obtained by using the total amount of 60 epochs. The left part of figure 5 shows c2 in the gray continuous line. In this curve, from 30 epochs forth c2 reaches 16%, and when using the total amount of epochs it decreases only 2% more.

Finally, the gray dashed line in the same figure shows the square root of the theoretical SNR as more epochs are considered and it is related to the right vertical axis. c1 was divided into two parts, from the first epoch to an epoch n , and from n to the end of c1. Then, two polynomial regressions were performed for each part of c1 using functions of the type $f(n) = c \cdot (n)^a$, where c is a scale parameter. The right part of figure 5 shows in the black line the a value of the first part of c1, as n varied. It can be seen that from 7 to 11 epochs the a value is quite close to the value of the SNR curve (that is 0.5).

The right part of figure 5 shows in the gray line the a value of the second part of c1, as n var-

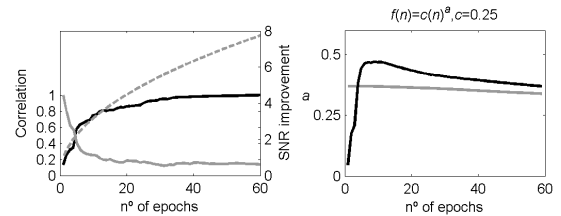


Figure 5: Left: c1 of channel C3 is shown in the black continuous line; c2 of channel C3 is shown in the gray continuous line; the \sqrt{SNR} curve is shown in the gray dashed line. Right: The a value of the first part of c1 is shown in the black line. The a value of the second part of c1 is shown in the gray line.

ied. The a value obtained from 11 to 60 epochs, corresponds to $a = 0.34$, which means approximately $f(n) = \sqrt[3]{n}$. This indicates that only for the first 10 epochs, where c1 reaches 80%, the information increases as predicted by the SNR curve. Then, most of the information about the ERD/ERS pattern is already retained with just 10 epochs.

As the polynomial regression obtained values very close to the SNR enhancement function, we assume that the non-converged part of c1 can represent the EEG SNR. Then, the application of *fastICA* algorithm would enhance a little the EEG SNR what should be verified from c1. In the same way, the use of *runica* algorithm would decrease the EEG SNR, what should be also verified from c1. The left part of figure 6 shows this relation where the black line shows c1 of channel C3 obtained without artifact removal, by only using the CAR method. The dark gray line shows c1 obtained with *fastICA* and the light gray line shows c1 obtained with *runica*.

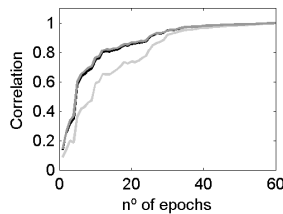


Figure 6: c1 of channel C3 is shown in the black line; c1 of channel C3 obtained with *fastICA* is shown in the dark gray line; c1 of channel C3 obtained with *runica* is shown in the light gray line.

5 Conclusion

In previous works we described our BCI and regarding the processing time we suggested the use of 1 s time windows with 50% of overlap (Benevides et al., 2011; Benevides et al., 2012). Then, the classification output is made every 0.5 s and all tested algorithms could be implemented online in BCI applications running minimally in our aforementioned requirements.

As BCI applications needs an online usage of ICA, the "unmixing" matrix \mathbf{W} can be estimated during some training trials and used in later trials, and the processing time will be only due the matrix multiplication. The *fastICA* algorithm obtained the best results and it is our suggestion for artifact removal.

Acknowledgments

The authors thank CAPES and CNPq for their financial support to this research.

References

Benevides, A. B., Bastos, T. F. and Filho, M. S. (2011). Design of a general brain-computer interface, *Revista Controle & Automacao* **22**(6): 638–646.

Benevides, A. B., Bastos, T. F. and Filho, M. S. (2012). Pseudo-online classification of mental tasks using kullback-leibler symmetric divergence, *Journal of Medical and Biological Engineering* **32**(6): 411–416.

Cincotti, F., Matia, D., Aloise, F., Bufalari, S., Astolfi, L., de Vico Fallani, F., Tocci, A., Bachi, L., Marciani, M. G., Gao, S., del R. Millan, J. and Babiloni, F. (2008). High resolution eeg techniques for brain-computer interfaces applications, *Journal of Neuroscience Methods* **167**: 31–42.

Croft, R. J. and Barry, R. J. (2000). Removal of ocular artifact from the eeg: a review, *Clinical Neurophysiology* **30**: 5–19.

del R. Millan, J., Renkens, F., Mourino, J. and Gerstner, W. (2004). Noninvasive brain-actuated control of a mobile robot by human eeg, *IEEE Transactions on Biomedical Engineering* **51**: 1026–1033.

Ferreira, A., Celeste, W. C., Cheein, F. A., Filho, T. F. B., Filho, M. S. and Carelli, R. (2008). Human-machine interfaces based on emg and eeg applied to robotic systems, *Journal of NeuroEngineering and Rehabilitation* **5**: 1–15.

Ford, M. R., Sands, S. and Lew, H. L. (2004). Overview of artifact reduction and removal in evoked potential and event-related potential recordings, *Physical Medicine and Rehabilitation Clinics of North America* **15**: 1–17.

Jung, T. P., Makeig, S., Westerfield, M., Townsend, J., Courchesne, E. and Sejnowski, T. J. (2000). Removal of eye activity artifacts from visual event-related potentials in normal and clinical subjects, *Clinical Neurophysiology* **111**: 1745–1758.

Jung, T. P., Makeig, S., Westerfield, M., Townsend, J., Courchesne, E. and Sejnowski, T. J. (2001). Analysis and visualization of single-trial event-related potentials, *Human Brain Mapping* **14**: 166–185.

Luck, S. J. (2005). *An Introduction to the Event-Related Potential Technique*, The Mit Press, Cambridge, MA, London.

McFarland, D. J., McCane, L. M., David, S. V. and Wolpaw, J. R. (1997). Spatial filter selection for eeg-based communication, *Electroencephalography and Clinical Neurophysiology* **103**: 386–394.

Muller, S. M. T., Celeste, W. C., Bastos, T. F. and Filho, M. S. (2010). Brain-computer interface based on visual evoked potentials to command autonomous robotic wheelchair, *Journal of Medical and Biological Engineering* **30**: 407–416.

Pfurtscheller, G. and da Silva, F. H. L. (1999). Event related eeg/meg synchronization and desynchronization: basic principles, *Clinical Neurophysiology* **110**: 1842–1857.

Wolpaw, J. R. (2007). Brain-computer interfaces as new pathways, *Journal of Physiology* **579**: 613–619.

Wolpaw, J. R., Birbaumer, N., McFarland, D. J., Pfurtscheller, G. and Vaughan, T. M. (2002). Brain-computer interfaces for communication and control, *Clinical Neurophysiology* **113**: 767–791.